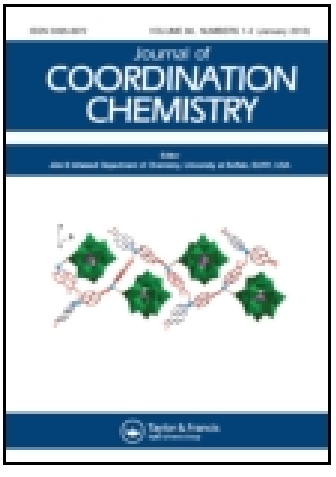

Journal of Coordination Chemistry
Publication details, including instructions for authors and subscription information:
http://www.tandfonline.com/loi/gcoo20

A new trans-dioxorhenium(V) complex with 4-aminopyridine: synthesis, structure, electrochemical aspects, DFT, and TD-DFT calculations

Arnab Bhattacharya[a], Smita Majumder[a], Jnan Prakash Naskar[b], Partha Mitra[c] & Shubhamoy Chowdhury[a]

[a] Department of Chemistry, Tripura University, Tripura, India

[b] Department of Chemistry, Inorganic Chemistry Section, Jadavpur University, Kolkata, India

[c] Department of Inorganic Chemistry, Indian Association for the Cultivation of Science, Kolkata, India

Published online: 29 Apr 2014.

To cite this article: Arnab Bhattacharya, Smita Majumder, Jnan Prakash Naskar, Partha Mitra & Shubhamoy Chowdhury (2014) A new trans-dioxorhenium(V) complex with 4-aminopyridine: synthesis, structure, electrochemical aspects, DFT, and TD-DFT calculations, Journal of Coordination Chemistry, 67:8, 1413-1428, DOI: 10.1080/00958972.2014.909590

To link to this article: http://dx.doi.org/10.1080/00958972.2014.909590

Journal of Coordination Chemistry, 2014
Vol. 67, No. 8, 1413–1428, http://dx.doi.org/10.1080/00958972.2014.909590

A new *trans*-dioxorhenium(V) complex with 4-aminopyridine: synthesis, structure, electrochemical aspects, DFT, and TD-DFT calculations

ARNAB BHATTACHARYA†, SMITA MAJUMDER†, JNAN PRAKASH NASKAR‡, PARTHA MITRA§ and SHUBHAMOY CHOWDHURY*†

†Department of Chemistry, Tripura University, Tripura, India
‡Department of Chemistry, Inorganic Chemistry Section, Jadavpur University, Kolkata, India
§Department of Inorganic Chemistry, Indian Association for the Cultivation of Science, Kolkata, India

(*Received 22 November 2013; accepted 27 February 2014*)

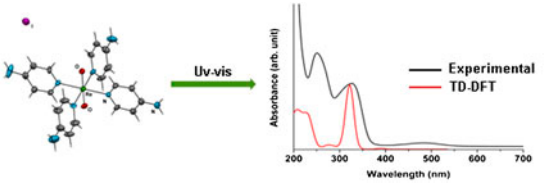

The reaction of 1 : 4.4 M proportion of *cis*-$[ReO_2I(PPh_3)_2]$ and 4-aminopyridine (ampy) in acetone–water gives *trans*-$[ReO_2(ampy)_4]I{\cdot}2H_2O$ (**1a**) in 85% yield. **1a** has been characterized by C, H, and N microanalyses, FT-IR, UV–vis, ^{1}H NMR spectroscopy, and molar conductivity. The X-ray crystal structure of **1a** reveals an octahedral *trans* dioxorhenium(V) complex with a "N_4O_2" coordination for rhenium. **1a** has an orthorhombic space group *C2221* with $a = 17.576(4)$, $b = 19.370(4)$, $c = 15.730(4)$ Å, $V = 5355(2)$ Å^3, and $Z = 8$. Geometry optimization of the *trans-O,O* complex, **1a** and its *cis-O,O* analog, **1b** performed at the level of density functional theory reveal that **1a** is more stable than **1b** by 25 kcal M^{-1} in the gas phase. The electronic spectrum of **1a** was also analyzed at the level of time-dependent density functional theory. Excitation of **1a** in methanol at 450 nm leads to a fluorescent emission at 505 nm with a quantum yield (Φ) of 0.04. Electrochemical studies of **1a** in acetonitrile show a quasi-reversible Re(V) to Re(VI) oxidation at 0.618 V *versus* Ag/AgCl. This redox potential matches with the calculated redox potential of 0.621 V *versus* Ag/AgCl.

Keywords: Dioxorhenium(V) complex; X-ray structure; Fluorescence; Electrochemistry; DFT and TD-DFT calculations

1. Introduction

Rhenium compounds encompass a major area in coordination chemistry. Rhenium compounds are potential candidates for diagnostic, as well as therapeutic purposes in nuclear medicine [1–3] and have also been studied for catalytic properties in oxidation,

*Corresponding author. Email: s.chowdhury@tripurauniv.in

de-oxygenation [4, 5], and hydrogenation reactions [6, 7]. Some rhenium compounds are potential photocatalysts for CO_2 reduction [8]. The coordination sites in most rhenium compounds having promising photophysical and photochemical properties invariably contain a tricarbonyl rhenium core with N donors like pyridine and triazole [9–11]. *Trans*-dioxorhenium(V) compounds are a well-known category of transition metal compounds with metal–ligand multiple bonds [12]. Their spectroscopic and photochemical properties have been summarized in a number of reviews [13, 14]. Some of these complexes show luminescence in the visible region. A promising example is $[ReO_2(py)_4]^+$, which displays a structured emission band between 590 and 750 nm [15]. To have a better understanding of the electronic and vibrational properties of such compounds, computational studies based on density functional theory (DFT) are areas of current research [16–20]. Gancheff *et al.* and Machura *et al.* have employed a standard combination of B3LYP with LANL2DZ in an effective way in their pursuit for optimizing and explaining spectral properties of rhenium compounds [21–24]. The chemical properties of various dioxorhenium(V) (ReO_2^+) complexes have been investigated as models for their application in radiopharmaceuticals [25, 26]. There is limited information pertaining to electrochemical properties in non-aqueous solutions for *trans* dioxorhenium(V) complexes, though they have potential *in vivo* importance [27]. Electrochemical reactions of *trans* dioxorhenium(V) complexes only with pyridine, bipyridine, or substituted pyridine and imidazole in acetonitrile (ACN) have been investigated by using cyclic voltammetry (CV) [28, 29]. The present work originates from the need for further studies on the basic chemistry of *trans* dioxorhenium(V) systems involving pyridine nitrogen donors to gain further insight into the electronic structures of such ligands and the corresponding *trans*-$[ReO_2]^+$ complexes. Herein, we report the structure of *trans*-$[ReO_2(ampy)_4]I\cdot 2H_2O$ (ampy = 4-aminopyridine) and the photophysical and electrochemical aspects. To gain further insight into the electronic structure, electronic transitions, and redox behavior, calculations at the level of DFT and time-dependent density functional theory (TD-DFT) were undertaken.

2. Experimental

2.1. *Materials and physical measurements*

Ammonium perrhenate and 4-aminopyridine (Sigma-Aldrich Chemicals) were used as received. The precursor *cis*-$[ReO_2I(PPh_3)_2]$ was prepared following a procedure reported earlier by Ciani *et al.* [30]. Microanalyses were performed with a Perkin-Elmer 2400II elemental analyzer. FT-IR spectra were recorded as KBr pellets with a Perkin-Elmer FTIR-100 spectrophotometer. UV–vis absorption spectra of the ligand and **1a** were recorded on a Perkin-Elmer Lambda 25 spectrophotometer and NMR spectra (in DMSO-d_6) with a Bruker DPX300 spectrometer. CV experiments were performed at 25 °C under nitrogen with a BAS Epsilon electrochemical workstation (Model CV-50). The measurements were carried out with a three-electrode assembly comprised of a BAS 11–2013 glassy carbon (GC) working electrode, a BAS 11-2025 reference electrode (Ag/AgCl) in TBAP/ACN solution and a BAS 51-2222 Pt wire auxiliary electrode. The working electrode was polished before each experiment with alumina slurry. All sample solutions were deoxygenated by purging with nitrogen for at least 10 min prior to each acquisition. All potentials reported herein are referenced to Ag/AgCl. The emission spectrum was recorded on a Shimadzu RF-5000

fluorescence spectrophotometer at room temperature (298 K) in degassed methanol. The fluorescence quantum yield (Φ) of the complex was determined using phenanthrene as a reference [31]. The complex and the reference dye were excited at the same wavelength maintaining nearly equal absorbance, and the emission spectra were recorded. The area of the emission spectrum was integrated and the quantum yield was calculated according to the following equation:

$$\Phi_S/\Phi_R = [A_S/A_R] \times [(Abs)_R/(Abs)_S] \times [\eta_S^2/\eta_R^2] \quad (1)$$

Here, Φ_S and Φ_R are the fluorescence quantum yields of the sample and the reference, respectively, A_S and A_R are the area under the fluorescence spectra of the sample and the reference, respectively, $(Abs)_S$ and $(Abs)_R$ are the respective optical densities of the sample and the reference solution at the wavelength of excitation and η_S and η_R are, respectively, the values of the refractive indices for the sample and the reference.

2.2. *Synthesis of trans-[ReO2(ampy)4]I·2H2O (1a)*

A mixture of *cis*-[$ReO_2I(PPh_3)_2$] (0.412 g, 0.50 mM) and 4-aminopyridine (0.207 g, 2.2 mM) in 30 mL acetone was stirred at room temperature for 15 min followed by addition of 2 mL of water. The dark orange solution was stirred for another 30 min and finally the reaction mixture was allowed to evaporate in the air. After three days, the separated crystalline product was collected by filtration, washed thoroughly with diethyl ether, and dried in a vacuum desiccator over fused $CaCl_2$. Yield: 0.322 g 85%, Anal. Calcd for $C_{20}H_{28}N_8O_4ReI$: C, 31.69; H, 3.73; N, 14.79. Found: C, 31.53; H, 3.65; N, 14.98. FT-IR (KBr/cm^{-1}): (C=N) 1635 (vs); (O=Re=O) 804 (m). ^{1}H NMR (DMSO-d_6, 300 Hz) (δ, ppm): 6.51 (d, J = 6.5 Hz, 8H, Ar); 6.65 (s, 8H, -NH_2); 8.12 (d, J = 7 Hz, Ar). UV–vis (CH_3OH), λ_{max}, nm (ε, $M^{-1}\,cm^{-1}$): 250 (25 365); 327 (17 385); 483 (1730). Λ_M (CH_3OH): 98 $\Omega^{-1}\,cm^2\,M^{-1}$ (1 : 1 electrolyte).

A moderately concentrated solution of this bulk compound in acetone was left for slow evaporation at room temperature to get dark red pyramidal crystals. The crystals were found to be suitable for X-ray crystallography.

2.3. *X-ray crystal structure analysis*

An appropriate single crystal of **1a** was mounted on a Bruker SMART APEX II CCD area detector diffractometer. Intensity data were collected at 293(2) K using graphite-monochromated Mo-K_α radiation (λ = 0.71073 Å). Intensity data of **1a** were reduced using SAINT [32] and the empirical absorption corrections were performed with SADABS [33]. The structure of **1a** was solved by direct methods and refined by full-matrix least-squares based on $|F|^2$ using SHELXL-97 [34]. All non-hydrogen atoms were refined anisotropically. Hydrogens were placed in calculated positions and constrained to ride on their parent. Even the best single crystal of **1a** selected for data collection gave diffuse diffraction spots, indicating a large mosaic spread. A few of the diffraction spots were overlapping and the integration of these spots could not be carried out properly by the processing software. Consequently, a small portion of the reflections collected was rejected and the structure was refined using the available data ($1.6 < \theta < 25.0°$), which was adequate to give a precise structure. All the calculations were carried out using SHELXS-97, SHELXL-97, and SHELXTL [34] programs. The crystallographic data for **1a** are summarized in table 1.

Table 1. Crystal data and structure refinement for **1a**.

Parameter	Complex **1a**
Formula	$C_{20}H_{24}N_8O_2ReI$, $2(H_2O)$
Formula weight	757.61
Crystal system	Orthorhombic
Space group	$C222_1$
Unit cell dimensions	
a (Å)	17.576(4)
b (Å)	19.370(4)
c (Å)	15.730(4)
Volume (Å^3)	5355(2)
Z	8
Temperature (K)	293(2)
ρ_{Calcd} (g/cm^3)	1.880
μ (Mo-K$_\alpha$) (mm^{-1})	5.731
F (0 0 0)	2912
Crystal size (mm)	0.09 × 0.14 × 0.20
λ (Mo-K$_\alpha$) (Å)	0.71073
θ ranges (°)	$1.6 < \theta < 25.0$
Total reflection	19,173
Reflection independent (R_{int})	4731 (0.109)
$h/k/l$	−20, 19/–23, 23/–18, 18
Reflection observed ($I > 2\sigma$)	3949
R_1	0.0525
wR_2	0.1315
Goodness of fit	1.00
$\Delta\rho_{max}$ and $\Delta\rho_{min}$ (e Å^{-3})	1.94, −1.69

$R_1 = \Sigma||F_o| - |F_c||/\Sigma|F_o|$, $wR_2 = [\Sigma w(F_o^2 - F_c^2)^2/\Sigma w(F_c^2)^2]^{1/2}$, Calcd $w = 1/[\sigma^2(F_o^2) + (0.064P)^2]$, where $P = (F_c^2 + 2F_o^2)/3$.

2.4. *Computational details*

The GAUSSIAN-09 Revision C.01 program package was used for all calculations [35]. The gas phase geometry of *trans-O,O* $[ReO_2(ampy)_4]^+$ (cation in **1a**) and *cis-O,O* $[ReO_2(ampy)_4]^+$ (cation in **1b**) were fully optimized without symmetry restriction in singlet ground states with the gradient-corrected DFT level coupled with Becke's exchange functional [36] including the correlation functional of Lee, Yang and Parr (B3LYP) [37]. The effective core potential with basis set LANL2DZ was employed for Re following the associated valence double ζ basis set of Hay and Wadt [38–40]. The calculations for hydrogen, carbon, nitrogen, and oxygen were found to be sufficiently accurate using MIDI basis set [41]. All the basis sets for computations in this study were obtained from basis set exchange software and the EMSL Basis Set Library [42, 43]. The electronic spectrum of the cation in **1a** was calculated with the TD-DFT method and the solvent effect (in methanol) was simulated using the polarizing continuum model with the integral equation formalism (C-PCM) [44–47]. For the cation in **1a**, 120 singlet–singlet spin-allowed excitations in solution were taken into account. For the determination of the Gibbs free energy, the same basis set and the same solvent model were considered.

3. Results and discussion

3.1. *Synthesis and formulation*

The synthesis of *trans*-tetrakis complexes of rhenium with pyridine and substituted pyridine analogs has been reported. One method employed heating of $[ReO_2I(PPh_3)_2]$ with pyridine

for 15 min to give $[ReO_2(py)_4]I$ [48]. The reaction of K_2ReCl_6 with O_2 in aqueous pyridine resulted in $[ReO_2(py)_4]Cl$, while in another run stirring of $[ReO_2I(PPh_3)_2]$ with 4-methoxypyridine in methanol followed by heating under reflux gave the desired substituted pyridine analog of $[ReO_2(py)_4]I$ [49, 50]. Again, synthesis of $[ReO_2(py)_4]Cl$ in good yield out of the refluxing of a mixture of $ReOCl_3(PPh_3)_2$ and pyridine in mixed solvents like water and acetone is also recommended [51]. Apart from these synthetic strategies, a recent method generates $[ReO_2(py)_4]I_3$ out of the reaction of Re(III) iodide with dry pyridine via refluxing [52].

In contrast to all the reported methods, we have synthesized **1a** in a modified route of a reported method [49]. In our case, the reaction of *cis*-$[ReO_2I(PPh_3)_2]$ with 4-aminopyridine at room temperature in acetone did not result in the *cis*-dioxo Re(V) complex, but *trans*-$[ReO_2(ampy)_4]I{\cdot}2H_2O$ in substantial yield. The reaction of 1 : 4.4 stoichiometric proportions of *cis*-$[ReO_2I(PPh_3)_2]$ and 4-aminopyridine in acetone–water and subsequent slow aerial evaporation of the mother liquor enabled us to isolate *trans*-$[ReO_2(ampy)_4]I{\cdot}2H_2O$ (**1a**) in good yield. In the solid state, **1a** is air-stable for several months, while in solution it lasts only 24 h. **1a** is soluble in acetone, methanol, ACN, and dimethyl sulfoxide. **1a** is diamagnetic. The molar electrical conductivity (98 $\Omega^{-1}\,cm^2\,M^{-1}$) of ~$10^{-3}$ M solution of **1a** in methanol indicates its 1 : 1 electrolytic nature in methanol [53].

3.2. *X-ray crystal structure*

The crystal structure of **1a** reveals that the asymmetric contains half of two tetrakis(4-aminopyridine)dioxorhenium(V) cations, an I^- and two waters. An ORTEP perspective of the asymmetric unit, along with the atom numbering scheme, is shown in figure 1. Selected metrical parameters for **1a** are given in table 2. The shape of the cation in **1a** can be linked to a four-blade propeller having the shaft at O=Re=O core. The geometry around Re is octahedral with four imino N atoms of 4-aminopyridine molecules coordinated to the equatorial plane of ReO_2^+. The bond lengths of Re=O are 1.78 and 1.75 Å, while the lengths of the Re–N bonds are in the range 2.12–2.18 Å. These Re=O and Re–N bond distances fall in the range typical for *trans*-dioxorhenium(V) complexes [24, 27, 54–60]. The two *trans*-oxo ligands are almost linear with O–Re–O angles of 176.6(4)° and 178.3(4)°. The ∠O–Re–N angles are around 90°, in the typical range for *trans*-dioxorhenium(V) complexes [24, 27, 49–55]. The crystal structure is stabilized by O–H···O, O–H···N, and N–H···O hydrogen bonds. The water molecules and the cations form intermolecular hydrogen bonds (table 3), giving a 3-D supramolecular network. The crystal packing diagram illustrating the hydrogen bonding in **1a** is shown in figure 2.

3.3. *Spectroscopic properties*

3.3.1. FT-IR and NMR spectroscopy. The FT-IR spectrum of **1a** displays a single (O=Re=O) asymmetrical stretch at 804 cm^{-1}. This band is typical (775–835 cm^{-1}) for ν_{as}(O=Re=O) [24, 27, 54, 61]. The characteristic ν(C=N) for the ampy ligand in **1a** can be discerned at 1616 and 1635 cm^{-1}. In free ampy, this C=N (pyridyl) vibration is at 1649 cm^{-1}. This lowering in wavenumber is due to the binding of C=N to Re. The experimental vibrational spectrum of **1a** was compared with the calculated (non-scaled) spectrum of **1a** (figure S1, see online supplemental material at http://dx.doi.org/10.1080/00958972.2014.909590). The calculated vibrational stretches of **1a** agree with the

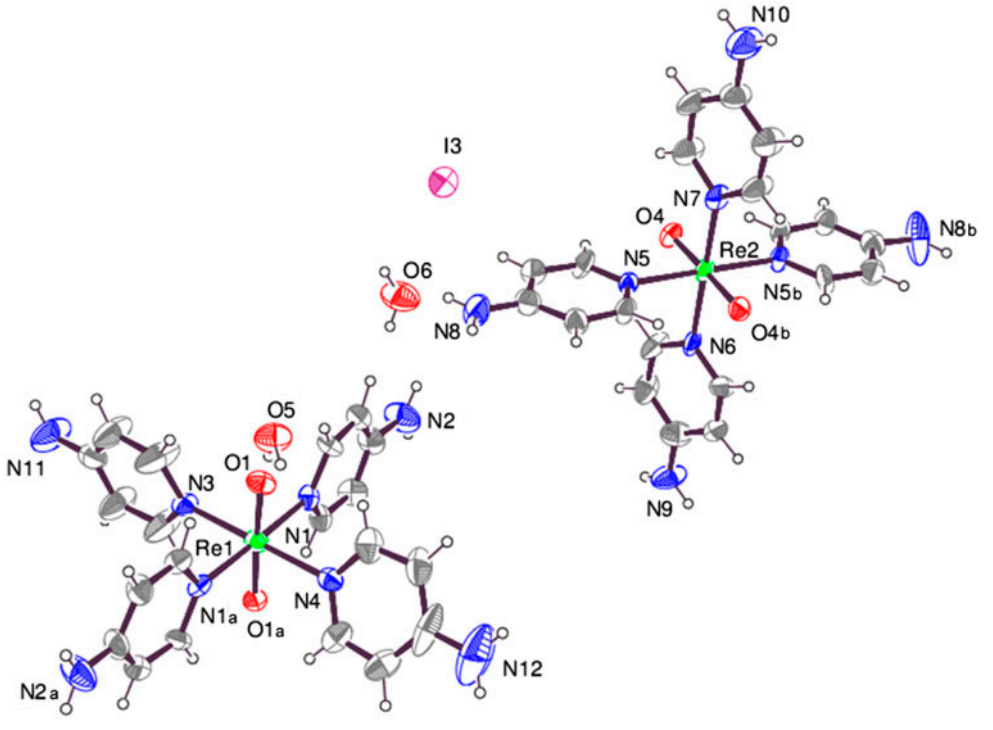

Figure 1. ORTEP view of **1a** showing the atom labeling scheme with 30% probability ellipsoids.

Table 2. Selected bond lengths and angles for **1a**.

Bond lengths/bond angles	Experimental	Bond lengths/bond angles	Experimental	Optimized
Re1–O1	1.778(7)	Re2–O4	1.753(8)	1.767
Re1–N1	2.117(9)	Re2–N5	2.153(8)	2.164
Re1–N3	2.141(14)	Re2–N6	2.161(16)	2.165
Re1–N4	2.176(14)	Re2–N7	2.110(14)	2.166
Re1–O1*a*	1.778(7)	Re2–O4*b*	1.753(8)	1.767
Re1–N1*a*	2.117(9)	Re2–N5*b*	2.153(8)	2.165
O1–Re1–N1	90.0(3)	O4–Re2–N5	88.8(3)	89.88
O1–Re1–N3	91.7(3)	O4–Re2–N6	89.2(3)	89.99
O1–Re1–N4	88.3(3)	O4–Re2–N7	90.8(3)	90.00
O1–Re1–O1*a*	176.6(4)	O4–Re2–O4*b*	178.3(4)	179.76
O1–Re1–N1*a*	90.1(3)	O4–Re2–N5*b*	91.2(3)	90.00
O1*a*–Re1–N1	90.1(3)	O4*b*–Re2–N5	91.2(3)	89.88
O1*a*–Re1–N3	91.7(3)	O4*b*–Re2–N6	89.2(3)	90.12
O1*a*–Re1–N4	88.3(3)	O4*b*–Re2–N7	90.8(3)	89.99
O1*a*–Re1–N1*a*	90.0(3)	O4*b*–Re2–N5*b*	88.8(3)	89.88
N1–Re1–N3	89.2(2)	N5–Re2–N6	89.6(3)	89.61
N1–Re1–N4	90.8(2)	N5–Re2–N7	90.4(3)	90.43
N1–Re1–N1*a*	178.4(3)	N5–Re2–N5*b*	179.3(4)	179.73
N3–Re1–N4	179.98(5)	N6–Re2–N7	180.00	179.96
N1*a*–Re1–N3	89.2(2)	N5*b*–Re2–N6	89.6(3)	89.84
N1*a*–Re1–N4	90.8(2)	N5b–Re2–N7	90.4(3)	90.12

Note: $a = -x, y, 3/2 - z$; $b = x, -y, -z$.

Table 3. Hydrogen bonds (Å, °) for **1a**.

D–H···A	D–H	H···A	D···A	∠D–H–A
O5–H105···O1	0.85	2.06	2.899(13)	170
O5–H205···O4	0.85	1.89	2.733(12)	170
O6–H106···N11	0.82	2.49	3.022(18)	124
O6–H206···O5	0.83	2.09	2.710(16)	131
N11–H11*a*···O6	0.86	2.18	3.022(18)	164
N11–H11*b*···O6	0.86	2.18	3.022(18)	164

Note: $a = -x, y, 3/2 - z$; $b = x, -y, -z$.

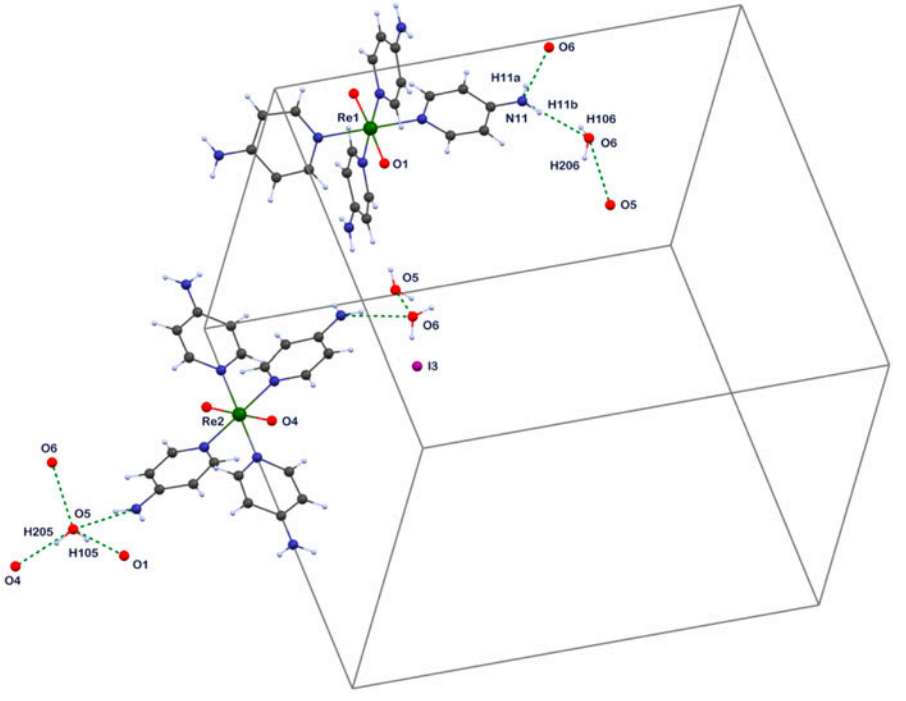

Figure 2. A view of packing diagram of **1a**, C gray, N blue, O red, I violet, and Re green (see http://dx.doi.org/10.1080/00958972.2014.909590 for color version).

experimental data. The experimental and calculated IR spectra of **1a** are similar in band positions and intensities. The calculated stretching frequency of 822 cm^{-1} for υ(O=Re=O) for **1a** is higher than its experimental value only by 2%. Likewise, the calculated stretching frequencies υ(C=N) of ampy at 1622 and 1695 cm^{-1} are higher than experimental values by ~0.4 and 3.6%. These marginal discrepancies are, however, justified when seen from a theoretical perspective. Often the computed gas phase data are at variance with the experimental data [62].

The ^{1}H NMR spectrum of **1a** in DMSO-d_6 displays sharp and distinct resonances, typical for diamagnetic d^2 metal ions like Re(V). In **1a**, the four-coordinated ampy ligands are magnetically equivalent. Consequently, the ligand protons in **1a** resonate in three signals – singlet, doublet, and doublet. In the ^{1}H NMR spectrum of **1a**, the signals due to amine protons and pyridyl ring protons can be found at 6.65, 6.51, and 8.12 ppm, respectively

(figure S2). The corresponding signals of free ampy can be assigned at 6.48, 6.03, and 7.99 ppm [63]. This downfield shift of the resonances in **1a** is due to coordination of four ampy ligands in the equatorial plane of the oxo-Re(V) core.

3.3.2. Electronic structure and spectrum. A schematic representation of the energy and character of the frontier orbitals of $[ReO_2(ampy)_4]^+$ is presented in figure 3. The energy gap from HOMO to LUMO is 3.947 eV. The highest occupied molecular orbital (HOMO) has significant metal character, predominantly d_{xz} with some contributions from ampy orbitals.

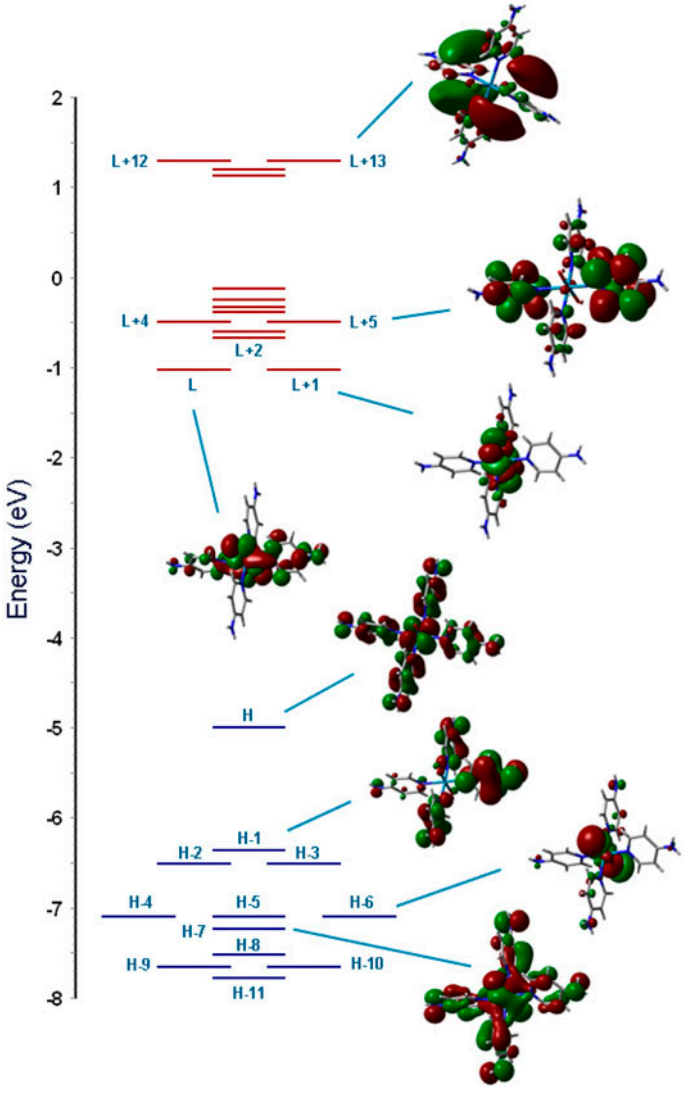

Figure 3. The energy (eV), character, and some contours of the unoccupied molecular orbitals of **1a**. Positive values of the orbital contour are represented in red (0.02 au) and negative values in green (–0.02 au) (see http://dx.doi.org/10.1080/00958972.2014.909590 for color version).

The highest occupied orbitals (HOMO-1 to HOMO-3) are more than 97% contributed by 4-aminopyridine orbitals. HOMO-4 to HOMO-6 is mostly composed by the p orbital of oxygen. The LUMO, LUMO + 1 orbitals are composed of d_{yz} and d_{xy} rhenium orbitals, respectively, in anti-bonding arrangement to oxygen *p* orbitals. These two LUMO orbitals contain mixed contributions from two 4-aminopyridine orbitals. To some extent they represent π-anti-bonding rhenium–oxygen molecular orbitals. Higher energy virtual MOs are contributed from π anti-bonding 4-aminopyridine orbitals. The lowest unoccupied molecular orbitals (LUMO + 2 to LUMO + 9) are mostly contributed by π-anti-bonding of ampy molecular orbitals. LUMO + 10 is mostly contributed by metal orbitals, d_{z2} and d_{x2-y2}.

The experimental and calculated electronic spectra of **1a** in methanol are presented in figure 4. Each calculated transition for $[ReO_2(ampy)_4]^+$ is represented by a Gaussian function. Table 4 summarizes the most important electronic transitions calculated at the TD-DFT level of theory. For the high energy part of the spectrum, only transitions with oscillator strength values larger than 0.0200 are included in table 4. Correlations of the calculated orbital excitations to the experimental bands were based on an overview of the contour plots and the magnitude of the relative energy to the occupied and unoccupied orbitals involved in the electronic transitions.

The experimental electronic spectrum of **1a** shows two absorptions (at 250 and 327 nm) in the UV region and one band at 483 nm in the visible range. This lowest energy band seems to be characteristic for *trans*-dioxorhenium(V) complexes and normally is assigned to the ligand field, $^1A_{1g}[(b_{2g})^2] \rightarrow {}^1E_g[(b_{2g})^1(e_g)^1]$ transition. For compounds like $[ReO_2(py)_4]^+$, $[ReO_2(3\text{-Cl-py})_4]^+$, $[ReO_2(3\text{-}SO_3\text{-py})_4]^+$, $[ReO_2(4\text{-MeO-py})_4]^+$, and $[ReO_2(impy)_4]^+$ – this absorption appears at 440, 428, 431, 448, and 455 nm, respectively [24, 64]. The TD-DFT/C-PCM calculations show that the lowest energy absorption band of **1a** (at 483 nm) originates from excitations between the HOMO and LUMO, LUMO + 1. As can be seen from figure 3, these orbitals are delocalized among rhenium and ampy orbitals. Taking into consideration the significant metallic character of HOMO, LUMO, and LUMO + 1 orbitals, these transitions may be considered as d–d transitions. The second lowest energy absorption band of **1a** (at 326 nm) originates from excitations between the HOMO and LUMO + 3, LUMO + 4 and LUMO + 5 (figure 3). These orbitals are

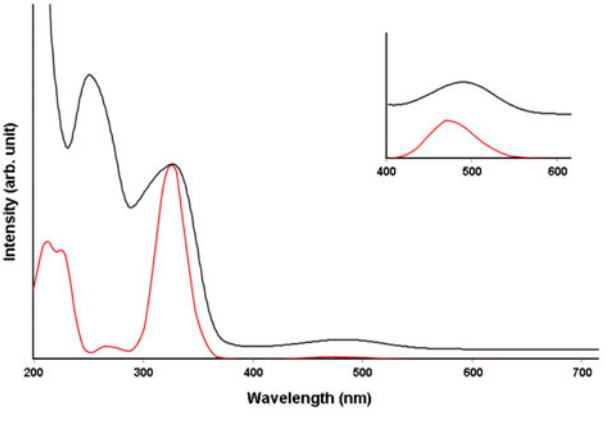

Figure 4. The experimental (black) and calculated (red) electronic absorption spectra of **1a** and magnified part is in inset (see http://dx.doi.org/10.1080/00958972.2014.909590 for color version).

Table 4. The energy and molar absorption coefficients of experimental absorption bands and electronic transitions calculated with the TD-DFT method for **1a**.

Most important orbital excitations	Character	λ [nm]	E [eV]	f	Experimental λ [nm] (E [eV]) ε
H→L+1	d/π(ampy)→d/π*(ampy)	479.08	2.588	0.0010	
H→L	d/π(ampy)→d/π*(ampy)	474.49	2.613	0.0093	483 (2.57) 1730
H→L+2	d/π(ampy)→π*(ampy)	338.61	3.662	0.0239	
H→L+3	d/π(ampy)→π*(ampy)	325.81	3.805	0.3952	326 (3.80) 17,385
H→L+4	d/π(ampy)→d/π*(ampy)	324.45	3.821	0.2974	
H→L+5	d/π(ampy)→π*(ampy)	323.08	3.838	0.0944	
H→L+6	d/π(ampy)→π*(ampy)	313.27	3.958	0.0616	
H→L+7	d/π(ampy)→π*(ampy)	307.32	4.034	0.0122	
H→L+8	d/π(ampy)→π*(ampy)	303.55	4.085	0.0207	
H-4→L+1	π(ampy)→d/π*(ampy)	289.04	4.290	0.0004	
H→L+10	d/π(ampy)→d/π*(ampy)	284.13	4.364	0.0016	
H→L+9	π(ampy)→d/π*(ampy)	281.50	4.404	0.0067	
H-6→L+1	π(ampy)→d/π^*(ampy)	277.84	4.462	0.0103	
H-6→L	d/π(ampy)→d/π*(ampy)	276.34	4.487	0.0146	
H-1→L	π(ampy)→d/π*(ampy)	262.92	4.716	0.0382	
H-1→L+3	π(ampy)→π*(ampy)	234.97	5.277	0.0635	
H-1→L+5	π(ampy)→π*(ampy)	231.96	5.345	0.0260	
H-2→L+3	π(ampy)→π*(ampy)	228.49	5.426	0.1038	250 (4.96) 25,365
H-1→L+4	π(ampy)→d/π*(ampy)	228.10	5.436	0.0384	
H-1→L+4	π(ampy)→d/π*(ampy)	225.62	5.495	1.0810	
H-1→L+6	π(ampy)→π*(ampy)				
H→L+12	d/π(ampy)→π*(ampy)	221.55	5.596	0.0273	
H→L+13	d/π(ampy)→π*(ampy)	220.29	5.628	0.0396	
H-1→L+7	π(ampy)→π*(ampy)	217.65	5.696	0.509	
H-3→L+7	π(ampy)→π*(ampy)	217.16	5.709	0.0270	
H-4→L+5	π(ampy)→π*(ampy)	212.01	5.848	0.1164	
H-1→L+9	π(ampy)→d/π*(ampy)				
H-6→L+4	π(ampy)→d/π*(ampy)	211.82	5.853	0.0298	
H-9→L	π(ampy)→d/π*(ampy)	210.42	5.892	0.1340	
H-2→L+9	π(ampy)→d/π*(ampy)	209.51	5.918	0.0540	
H-3→L+9	π(ampy)→d/π*(ampy)	206.10	6.016	0.1009	
H-5→L+7	π(ampy)→π*(ampy)	204.99	6.048	0.0222	
H-7→L+3	d/π(ampy)→π*(ampy)	201.04	6.139	0.0424	
H-5→L+9	π(ampy)→d/π*(ampy)	201.04	6.167	0.0209	
H-7→L+5	d/π(ampy)→π*(ampy)	200.45	6.185	0.0212	

Notes: ε – molar absorption coefficient [$dm^3\ M^{-1}\ cm^{-1}$]; f – oscillator strength; H – highest occupied molecular orbital; L – lowest unoccupied molecular orbital.

delocalized among rhenium and ampy orbitals. Since the underlying orbitals are of mixed type owing to their delocalization, this second lowest energy transition in **1a** can be assigned as metal–ligand to ligand charge transfer transition. The origin of the absorption band at the highest energy part of the spectrum (at 250 nm) is attributed to ligand to ligand charge transfer since most of the transitions with good oscillator strengths in this region contribute to the $\pi \rightarrow \pi^*$ of ampy.

3.3.3. Emission spectroscopy. The emission spectrum was recorded in deaerated methanol of **1a** at room temperature. The most intense and representative emission spectrum was obtained with 450 nm excitation wavelength (figure 5) and the consequent emission band centered at 505 nm. The observed emission band is broad and shows no vibronic structure. In general the band position, multiplicity and emission quantum yield are strongly dependent on the structure and rigidity of the underlying complex. The fluorescence quantum

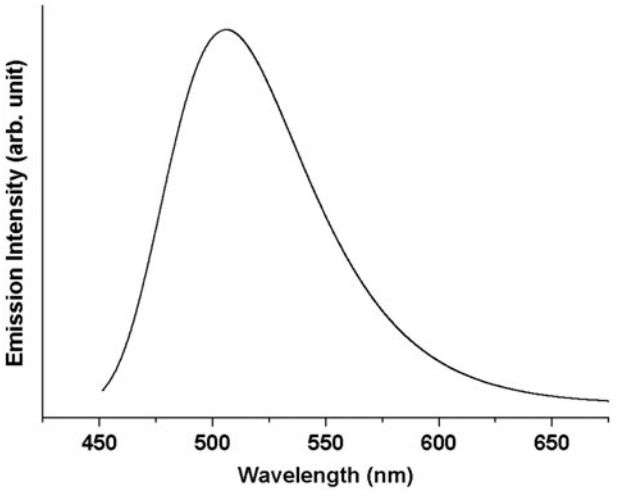

Figure 5. The fluorescence spectrum of **1a** in methanol obtained upon excitation at 450 nm.

yield (Φ) of **1a** was 0.04. The excitation spectrum of **1a** monitored at 505 nm showed a broad band at ca. 305–430 nm. With reference to previous spectroscopic work on this class of compounds, the present emission in **1a** originates most likely from $(d_{xy})^1(d_{xz})^1$ [$^3B_{3g}$] and $(d_{xy})^1(d_{yz})^1$ [$^3B_{2g}$] triplet excited states [65–68].

3.4. *Geometry optimization*

Optimizations starting from the crystallographically determined molecular structure of **1a** lead to a minimum as stationary point. Selected optimized parameters are tabulated in table 2. The general trends observed in the crystal data are well reproduced in the optimizations. The calculated bond lengths of Re=O deviate by –0.011 Å and +0.014 Å, while the Re–N bond lengths deviate from the experimental results by –0.010 to +0.056 Å. The calculated bond angles are in agreement with the observed experimental data. In general, a marginal deviation of the calculated bond parameters from the experimental values is noticed. This discrepancy may arise from the basis sets which were approximated during calculation or may be due to the influence of the crystal packing on the values of the experimental bond lengths [19, 62, 69]. The theoretical calculations do not consider the effects of the chemical environment.

To elucidate the bonding and electronic properties of *trans-O,O* (**1a**) and *cis-O,O* (**1b**) cations (scheme 1), we have used calculations based on DFT. The geometries were optimized in the singlet state using the DFT method (B3LYP in combination of LANL2DZ). From the geometry optimizations of the isomers, *trans-O,O* (**1a** cation) is more stable than *cis-O,O* (**1b** cation) by 25 kcal M^{-1}. Here, we isolate and crystallize **1a**. Thus, it can be concluded that the theoretical outcomes and the experimental observations are in harmony.

3.5. *Electrochemistry*

The redox properties of **1a** are examined in ACN at GC electrode under N_2. **1a** exhibits a redox couple on the positive side of the Ag/AgCl reference electrode. The CV of **1a**

(figure 6) shows a quasi-reversible voltammogram at 0.618 V *versus* Ag/AgCl. The corresponding peak current ratio, i_{pa}/i_{pc} is 1.16 with peak-to-peak separation, ΔE of 71 mV. The, 4-aminopyridine is electrochemically inert in the potential range of interest, i.e. on the positive side of the Ag/AgCl. Thus, this oxidation can safely be assigned as metal centered. Comparison of the voltammetric peak currents with those of the ferrocene–ferrocenium couple under the same experimental condition establishes that the oxidative response in **1a** involves one electron which is ascribed to the $Re^{(VI)}/Re^{(V)}$ couple [25, 66, 70]. The electrochemical data for **1a** is tabulated in table 5. In general, the peak current, i_p, increases with the square root of scan rate ($v^{1/2}$) but not in proportionality. Thus, the metal centered oxidation for **1a** is quasi-reversible [24]. The electrochemical response for **1a** can be assigned as:

$$Re^{VI}O_2(4\text{-ampy})_4]^{2+} + e^- \rightarrow [Re^{V}O_2(4\text{-ampy})_4]^{+} \tag{2}$$

The electrochemical behavior of **1a** can be rationalized through DFT calculation. The contribution of the rhenium to the occupied MOs is significant. Thus, **1a** shows predominant metal-based oxidation, enabling us to determine the Gibb's free energy theoretically which in turn leads to prediction of reduction free energy of **1a**. In doing so, the Born–Haber thermodynamic cycle was framed. The free energies of the oxidized, as well as the reduced forms of **1a** in the gas phase and also in solution (scheme 2) were incorporated in this cycle. The estimated reduction free energy was then referenced with respect to the standard hydrogen electrode (SHE).

If the above thermodynamic cycle is used for prediction of reduction free energies, then the standard state corrections are redundant since the number of moles of reactants in the left-hand side and the number of moles of products on the right-hand side are the same. From the above cycle, the following equations may be written:

$$\Delta G^{VI/V}_{red(ACN)} = \Delta G^{VI/V}_{red(g)} + \Delta\Delta G_{solv} \tag{3a}$$

$$\Delta\Delta G_{solv} = \Delta_s G_{reduced(ACN)} - \Delta_s G_{oxidized(ACN)} \tag{3b}$$

$$\Delta G_{red} = \Delta G^{VI/V}_{red(ACN)} - \Delta G_{red(Ref.electrode)} \tag{3c}$$

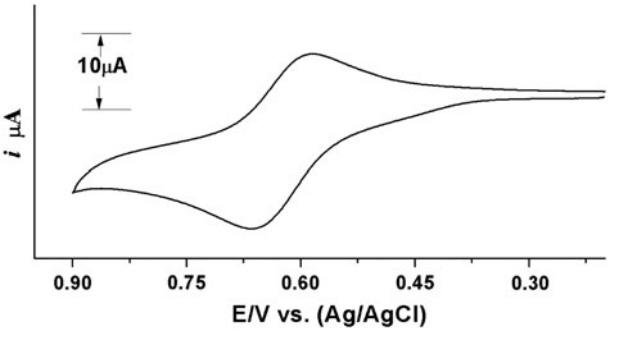

Figure 6. CV of **1a** in ACN at a scan rate of 100 mVs^{-1}. The analyte concentration was 0.982×10^{-3} M.

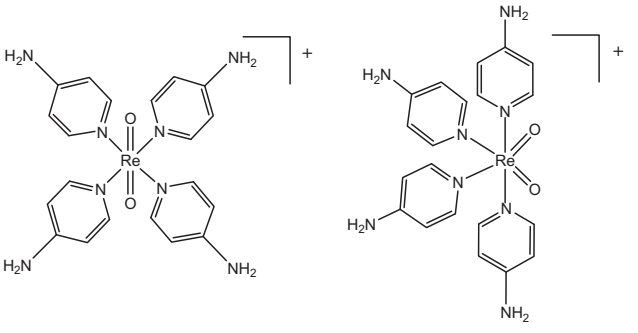

trans-O, O (**1a** cation) *cis-O, O* (**1b** cation)

Scheme 1.

where $\Delta G^{VI/V}{}_{red(g)}$ is the reduction free energy of **1a** in the gas phase, $\Delta_s G_{reduced(ACN)}$ and $\Delta_s G_{oxidized(ACN)}$ are the solvation free energies of the reduced and oxidized forms of the complex, respectively, and $\Delta\Delta G_{solv}$ is the difference between the solvation free energies of the reduced and the oxidized complexes, i.e. $(\Delta_s G_{reduced(ACN)} - \Delta_s G_{oxidized(ACN)})$. The absolute reduction free energy for the Re(VI) to Re(V) reduction, $\Delta G^{VI/V}{}_{red(ACN)}$, was determined by using equation (3a), then equation (3c) was used to obtain a reduction free energy of a reference electrode. The reference electrode considered here for solution is the SHE. In the present calculation, the absolute reduction free energy value of SHE was considered as 4.28 eV. This value has recently been evaluated based on the thermodynamic data of a proton by Truhlar *et al.* [71]. Subsequently the reduction potential value was evaluated from the predetermined ΔG_{red} value employing the standard relationships, $E_{1/2} = -\Delta G_{red}/(nF)$, where n is the number of electrons transferred and F is the Faraday constant [72]. We have determined the reduction free energy ($\Delta G^{VI/V}{}_{red(ACN)}$) through DFT by using the solvent model, C-PCM and the obtained value is –5.11 eV. In our present endeavor, the calculated $E_{1/2}$ is 0.830 V *versus* SHE. After necessary reference conversion, this value comes out as 0.621 V *versus* Ag/AgCl. Thus, the theoretical outcome agrees fairly well with our experimental redox potential, 0.618 V *versus* Ag/AgCl.

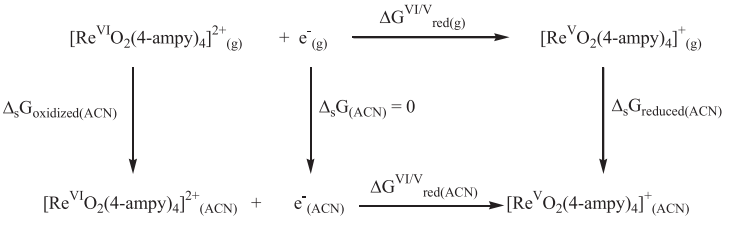

Scheme 2. Proposed thermodynamic cycle for the prediction of reduction free energy ($\Delta G^{VI/V}_{red}$).

Table 5. CV data for **1a**.

Entry	E_{pa} (i_{pa})	E_{pc} (i_{pc})	ΔE	$E_{½}$	i_{pa}/i_{pc}
1a	0.653 (10.94)	0.582 (9.46)	71	0.6175	1.16

Notes: E_{pa} = anodic peak potential, *V*; E_{pc} = cathodic peak potential, *V*; i_{pa} = anodic peak current, μA; i_{pc} = cathodic peak current, μA; $\Delta E = (E_{pa} \sim E_{pc})$ mV, $E_{½} = 0.5(E_{pc} + E_{pa})$ *V*.

4. Conclusion

We have synthesized and characterized a dioxorhenium(V) complex from 4-aminopyridine (ampy). The X-ray crystal structure of $[Re^{V}O_2(ampy)_4]I{\cdot}2H_2O$ (**1a**) reveals that the rhenium(V) is octahedral "N_4O_2". The two oxygen donors are *trans*. Thus, **1a** can be described as a *trans-O,O* dioxorhenium(V) complex. DFT calculations in the gas phase reveal that the *trans-O,O* dioxorhenium(V) complex, **1a** is more stable than the *cis* counterpart, *cis-O,O* dioxorhenium(V) complex, **1b** by 25 kcal M^{-1}. The electronic structure of **1a** has also been studied by C-PCM solvent model (methanol) employing DFT level of theory and the outcome is in good agreement with the experimental data. **1a** also displays a luminescence emission at 505 nm upon excitation at 450 nm. In CV, **1a** undergoes a quasi-reversible one electron oxidation from Re(V) to Re(VI) in ACN at 0.618 V *versus* Ag/AgCl. The redox potential value was also determined through DFT. The calculated potential, 0.621 V *versus* Ag/AgCl, nicely corroborates our experimental redox potential.

Supplementary material

Crystallographic data for the structural analyses have been deposited with the Cambridge Crystallographic Data Centre (CCDC No. 913368). Copies of this information can be obtained free of charge from The Director, CCDC, 12 Union Road, Cambridge, CB2 1EZ, UK (Fax: +44 1223 336033; E-mail: deposit@ccdc.cam.ac.uk or http://www.ccdc.cam.ac.uk).

Acknowledgements

Financial support (Project No. SR/FT/CS-75/2010) from the SERC under Department of Science and Technology, New Delhi, India is gratefully acknowledged. J.P. Naskar gratefully acknowledges the University Grants Commission (UGC), New Delhi, India for financial support [F. No. 41-220/2012 (SR)].

References

[1] S. Liu. *Chem. Soc. Rev.*, **33**, 445 (2004).
[2] S.P. Fricker. *Metallomics*, **2**, 366 (2010).
[3] W.A. Volkert, T.J. Hoffman. *Chem. Rev.*, **99**, 2269 (1999).
[4] T.J. Korstanje, R.J.M.K. Gebbink. In *Topics in Organometallic Chemistry*, M.A.R. Meier, B.M. Weckhuysen, P.C.A. Bruijnicx (Eds), Vol. 39, pp. 129–174, Springer, Berlin Heidelberg (2012).
[5] S.C.A. Sousa, A.C. Fernandes. *Tetrahedron Lett.*, **52**, 6960 (2011).
[6] A. Landwehr, B. Dudle, T. Fox, O. Blacque, H. Berke. *Chem. Eur. J.*, **18**, 5701 (2012).
[7] J. Yi, S. Liu, M.M. Abu-Omar. *ChemSusChem.*, **5**, 1401 (2012).
[8] H. Takeda, O. Ishitani. *Coord. Chem. Rev.*, **254**, 346 (2010).
[9] P. Mondal, A. Hens, S. Basak, K.K. Rajak. *Dalton Trans.*, 1536 (2013).
[10] A. Seridi, M. Wolff, A. Boulay, N. Saffon, Y. Coulais, C. Picard, B. Machura, E. Benoist. *Inorg. Chem. Commun.*, **14**, 238 (2011).
[11] T.Y. Kim, A.B.S. Elliott, K.J. Shaffer, C.J. McAdam, K.C. Gordon, J.D. Crowley. *Polyhedron*, **52**, 1391 (2012).
[12] W.A. Nugent. J.M. Mayer, *Metal–Ligand Multiple Bonds*, Wiley, New York (1988).
[13] V.W.W. Yam, C.-M. Che. *Coord. Chem. Rev.*, **97**, 93 (1990).
[14] B. Machura. *Coord. Chem. Rev.*, **249**, 591 (2005).
[15] J.R. Winkler, H.B. Glay. *Inorg. Chem.*, **24**, 346 (1995).

[16] S. Michalik, J.G. Małecki, R. Kruszynski, V. Kozik, J. Kusz, M. Krompiec. *J. Coord. Chem.*, **64**, 2202 (2011).
[17] H. Xia, F. Zhao, W. Liu, Y. Wang. *J. Organomet. Chem.*, **727**, 10 (2013).
[18] S. Michalik. *J. Coord. Chem.*, **65**, 1189 (2012).
[19] S. Majumder, A. Bhattacharya, J.P. Naskar, P. Mitra, S. Chowdhury. *Inorg. Chim. Acta*, **399**, 166 (2013).
[20] S. Majumder, J.P. Naskar, S. Banerjee, A. Bhattacharya, P. Mitra, S. Chowdhury. *J. Coord. Chem.*, **66**, 1178 (2013).
[21] J.S. Gancheff, P.A. Denis, F.E. Hahn. *J. Mol. Struct.: THEOCHEM*, **941**, 1 (2010).
[22] J.S. Gancheff, P.A. Denis, F.E. Hahn. *Spectrochim. Acta Part A: Mol. Biomol. Spectrosc.*, **76**, 348 (2010).
[23] J.S. Gancheff, R.Q. Albuquerque, A. Guerrero-Martinez, T. Pape, L.D. Cola, F.E. Hahn. *Eur. J. Inorg. Chem.*, **2009**, 4043 (2009).
[24] B. Machura, M. Wolff, D. Tabak, Y. Ikeda, K. Hasegawa. *Polyhedron*, **39**, 76 (2012).
[25] D.H. Johnston, C.-C. Cheng, K.J. Campbell, H.H. Thorp. *Inorg. Chem.*, **33**, 6388 (1994).
[26] M.F. Cerdá, E. Méndez, G. Obal, C. Kremer, J.S. Gancheff, A.M.C. Luna. *J. Inorg. Biochem.*, **98**, 238 (2004).
[27] A. Canlier, T. Kawasaki, S. Chowdhury, Y. Ikeda. *Inorg. Chim. Acta*, **363**, 1 (2010).
[28] H.H. Thorp, J.V. Houten, H.B. Gray. *Inorg. Chem.*, **28**, 889 (1989).
[29] M.S. Ram, L.M. Skeens-Jones, C.S. Johnson, X.L. Zhang, C. Stern, D.I. Yoon, D. Selmarten, J.T. Hupp. *J. Am. Chem. Soc.*, **117**, 1411 (1995).
[30] G.F. Ciani, G. D'Alfonso, P.F. Romiti, A. Sironi, M. Freni. *Inorg. Chim. Acta*, **72**, 29 (1983).
[31] W.R. Dawson, M.W. Windsor. *J. Phys. Chem.*, **72**, 3251 (1968).
[32] SAINT Plus. *Data Reduction and Correction Program (Version 6.01)*, Bruker AXS, Madison, WI (1998).
[33] SADABS v. 2.01. *Bruker/Siemens Area Detector Absorption Correction Program*, Bruker AXS, Madison, WI (1998).
[34] G.M. Sheldrick. *Acta Crystallogr. Sect. A*, **64**, 112 (2008).
[35] M.J. Frisch, G.W. Trucks, H.B. Schlegel, G.E. Scuseria, M.A. Robb, J.R. Cheeseman, G. Scalmani, V. Barone, B. Mennucci, G.A. Petersson, H. Nakatsuji, M. Caricato, X. Li, H.P. Hratchian, A.F. Izmaylov, J. Bloino, G. Zheng, J.L. Sonnenberg, M. Hada, M. Ehara, K. Toyota, R. Fukuda, J. Hasegawa, M. Ishida, T. Nakajima, Y. Honda, O. Kitao, H. Nakai, T. Vreven, J.A. Montgomery, Jr., J.E. Peralta, F. Ogliaro, M. Bearpark, J.J. Heyd, E. Brothers, K.N. Kudin, V.N. Staroverov, R. Kobayashi, J. Normand, K. Raghavachari, A. Rendell, J.C. Burant, S.S. Iyengar, J. Tomasi, M. Cossi, N. Rega, J.M. Millam, M. Klene, J.E. Knox, J.B. Cross, V. Bakken, C. Adamo, J. Jaramillo, R. Gomperts, R.E. Stratmann, O. Yazyev, A.J. Austin, R. Cammi, C. Pomelli, J.W. Ochterski, R.L. Martin, K. Morokuma, V.G. Zakrzewski, G.A. Voth, P. Salvador, J.J. Dannenberg, S. Dapprich, A.D. Daniels, Ö. Farkas, J.B. Foresman, J.V. Ortiz, J. Cioslowski, D.J. Fox. *Gaussian 09, Revision C.01*, Gaussian Inc., Wallingford, CT (2009).
[36] A.D. Becke. *Phys. Rev. A*, **38**, 3098 (1988).
[37] C. Lee, W. Yang, R.G. Parr. *Phys. Rev. B*, **37**, 785 (1988).
[38] P.J. Hay, W.R. Wadt. *J. Chem. Phys.*, **82**, 270 (1985).
[39] P.J. Hay, W.R. Wadt. *J. Chem. Phys.*, **82**, 284 (1985).
[40] P.J. Hay, W.R. Wadt. *J. Chem. Phys.*, **82**, 299 (1985).
[41] R.E. Easton, D.J. Giesen, A. Welch, C.J. Cramer, D.G. Truhlar. *Theor. Chem. Acc*, **93**, 281 (1996).
[42] D. Feller. *J. Comput. Chem.*, **17**, 1571 (1996).
[43] K.L. Schuchardt, B.T. Didier, T. Elsethagen, L. Sun, V. Gurumoorthi, J. Chase, J. Li, T.L. Windus. *J. Chem. Inf. Model.*, **47**, 1045 (2007).
[44] V. Barone, M. Cossi. *J. Phys. Chem. A*, **102**, 1995 (1998).
[45] Y. Takano, K.N. Houk. *J. Chem. Theor. Comput.*, **1**, 70 (2004).
[46] J. Tomasi, B. Mennucci, R. Cammi. *Chem. Rev.*, **105**, 2999 (2005).
[47] C. Maurizio, R. Nadia, S. Giovanni, B. Vincenzo. *J. Comput. Chem.*, **24**, 669 (2003).
[48] M. Freni, D. Giusta, P. Romiti, G. Minghetti. *Gazz. Chim. Ital.*, **99**, 286 (1969).
[49] J.C. Brewer, H.B. Gray. *Inorg. Chem.*, **28**, 3334 (1989).
[50] J.H. Beard, J. Casey, R.K. Murmann. *Inorg. Chem.*, **4**, 797 (1965).
[51] M.S. Ram, J.T. Hupp. *Inorg. Chem.*, **30**, 130 (1991).
[52] M. Siczek, M.S. Krawczyk, T. Lis. *Acta Cryst.*, **E65**, m1057 (2009).
[53] W.J. Geary. *Coord. Chem. Rev.*, **7**, 81 (1971).
[54] S. Belanger, A.L. Beauchamp. *Inorg. Chem.*, **35**, 7836 (1996).
[55] G. Bandoli, A. Dolmella, T.I.A. Gerber, D. Luzipo, J.G.H. Du Preez. *Inorg. Chim. Acta*, **325**, 215 (2001).
[56] T. Kawasaki, A. Canlier, S. Chowdhury, Y. Ikeda. *Acta Cryst.*, **E66**, m857 (2010).
[57] K.R. Reddy, Ñ. Domingos, A. Paulo, I. Santos. *Inorg. Chem.*, **38**, 4278 (1999).
[58] R.L. Luck, R.S. O'Neill. *Polyhedron*, **20**, 773 (2001).
[59] A. Kochel. *Acta Cryst.*, **E62**, m1740 (2006).
[60] J.S. Gancheff, C. Kremeer, O.N. Ventura, S. Domínguez, C. Bazzicalupi, A. Bianchi, L. Suescun, A.W. Mombrú. *New J. Chem.*, **30**, 1650 (2006).
[61] A.M. Lebuis, J.M.C. Young, A.L. Beanchamp. *Inorg. Chem.*, **35**, 7836 (1996).

[62] B. Machura, R. Kruszynski, J. Kusz. *Polyhedron*, **27**, 1679 (2008).
[63] http://www.hanhonggroup.com/nmr/nmr_en/B61017.html
[64] M.S. Ram, L.M. Jones, H.J. Ward, Y.H. Wong, C.S. Johnson, P. Subramanian, J.T. Hupp. *Inorg. Chem.*, **30**, 2928 (1991).
[65] V.W.W. Yam, K.K. Tam, M.C. Cheng, S.M. Peng, Y. Wang. *J. Chem. Soc, Dalton Trans.*, 1717 (1992).
[66] V.W.W. Yam, Y.L. Pui, K.M.C. Wong, K.K. Cheung. *Inorg. Chim. Acta*, **300–302**, 721 (2000).
[67] C. Savoie, C. Reber. *Coord. Chem. Rev.*, **171**, 387 (1998).
[68] S. Sen, T. Mukherjee, S. Sarkar, S.K. Mukhopadhyay, P. Chattopadhyay. *Analyst*, **136**, 4839 (2011).
[69] B. Machura, M. Wolff, I. Gryca. *Polyhedron*, **30**, 142 (2011).
[70] M.S. Ram, C.S. Johnson, R.L. Blackbourn, J.T. Hupp. *Inorg. Chem.*, **29**, 238 (1990).
[71] C.P. Kelly, C.J. Cramer, D.G. Truhlar. *J. Phys. Chem. B*, **111**, 408 (2006).
[72] L.E. Fernandez, S. Horvath, S. Hammes-Schiffer. *J. Phys. Chem. C*, **116**, 3171 (2012).